Table 1. Patient characteristics (n = 130)

Characteristic	All patients	Range	LBRT (n = 64)	WBRT (n = 66)	p
Age (y)	58	24–87	58 (38–87)	58 (24–79)	.35
Karnofsky performance status	70	40–100	70 (40–100)	70 (40–100)	.35
RPA class	II	I–III	II (I–III)	II (I–III)	.78*
I	40	30.8	19	21	
II	55	42.3	26	29	
III	35	26.9	19	16	
Cancer type (%)					.96*
Lung cancer	55	42.3	29	26	
Non–small-cell lung cancer	54		29	25	
Small-cell lung cancer	1		0	1	
Breast cancer	18	13.8	9	9	
Colorectal cancer	14	10.8	6	8	
Skin cancer	6	4.6	3	3	
Other	37	28.5	17	20	
Diameter of brain tumor (mm)	38	10–65	38 (10–65)	38 (15–60)	.57
Removal status					.11
Gross total removal	124	95.4	59	65	
Partial removal	6	4.6	5	1	

Abbreviations: RPA = recursive partitioning analysis; WBRT = whole brain radiotherapy; LBRT = local brain radiotherapy,
Data presented as median, with range in parentheses.
* Chi-square test.

institutions in Japan (15). LBRT delivered by linear accelerator to the tumor bed with a margin determined using the two-field technique (opposing portal irradiation) according to a dose-fractionated schedule had been applied for the treatment of single brain metastasis after surgical removal at the National Cancer Center Hospital before September 2004. This was based on the ethics that we presumed we could treat intracranial relapse using stereotactic RT after LBRT. After discussion with neurosurgeons, radio-oncologists, and medical oncologists, however, the treatment policy was changed. WBRT has been used for the treatment of all patients with single brain metastasis after tumor removal since October 2004. A Phase I-II clinical trial of postoperative LBRT was reported, and the investigators concluded that LBRT was not a suitable substitute for WBRT (16). However, that previous study included only 12 patients, and 7 of these patients died of intracranial tumor progression. The median survival time was 7.2 months, similar to that after WBRT. Another retrospective study implied that LBRT might have a similar benefit to that of WBRT in patients with a single brain metastasis (17). Bahl *et al.* (18) reported 7 cases of postoperative LBRT, of which 4 cases recurred at the same site. These studies included only a small number of patients, and any conclusions regarding the clinical outcome of postoperative LBRT, especially compared with that of postoperative WBRT, are thus difficult to make. In the present analysis, we retrospectively compared the clinical outcomes of patients with a single brain metastasis who received surgery followed by either WBRT or LBRT.

PATIENTS AND METHODS

Patient population

From the database of the neurosurgery division at the National Cancer Center Hospital, we identified patients who had undergone brain tumor removal followed by RT between 1990 and 2008. The patients were included in the present analysis if they met the following criteria: age ≥18 years, a single brain metastasis identified by magnetic resonance imaging, and tumor removal followed by either WBRT or LBRT. The exclusion criteria were as follows: extracranial malignant lymphoma or hematological tumor; brain biopsy only; previous brain RT; surgery followed by observation, with brain RT once progression was recognized; and postoperative gamma knife or linear accelerator-based radiosurgery. All the patients who received LBRT (n = 64) were treated before October 2004, and all the patients who received WBRT (n = 66) were treated after October 2004.

Data collection and definitions of terms

All the medical charts for the eligible patients were reviewed. To compare the clinical outcomes of postoperative WBRT and LBRT, we collected the following data:; preoperative magnetic resonance imaging; date of surgery and RT; RPA classification before surgery; Karnofsky performance status (KPS) at presentation; primary tumor site; date of recognition of local recurrence or intracranial new metastases; patterns of progression; leptomeningeal metastasis development; date of death; and neurologic cause of death. For the additional evaluation of long-term survivors (≥2 years after surgery), we also reviewed the KPS at 2 years after surgery.

Local recurrence was defined as recurrence at the surgical site. Intracranial new metastases included the detection of new brain metastases other than those occurring at the surgical site or the development of leptomeningeal metastases. Leptomeningeal metastases were diagnosed using a cytologic examination of cerebrospinal fluid.

Surgery and RT

The surgical indications for single brain metastasis were generally as follows: tumor diameter ≥30 mm or a tumor diameter of <30 mm with neurologic dysfunction.

Whole brain RT was administered through two lateral ports covering the brain and meninges to the foramen magnum. Normally, WBRT was delivered using a 4-MV or 6-MV linear accelerator at

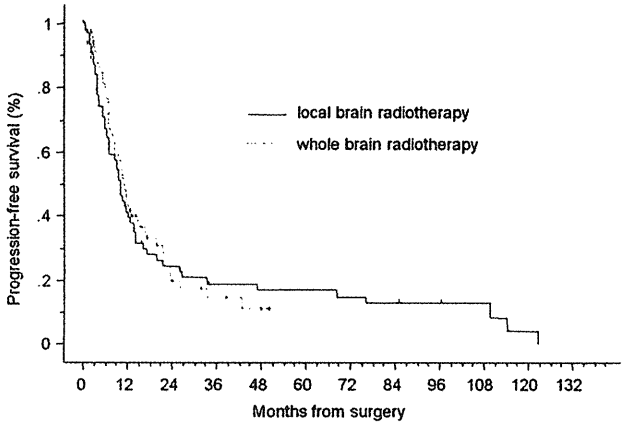

Fig. 1. Progression-free survival for patients with local brain radiotherapy (black line) and whole brain radiotherapy (dashed line).

a total dose of 30 Gy in 10 fractions or 37.5 Gy in 15 fractions. Patients who received LBRT underwent computed tomography simulation in the supine position. The clinical target volume consisted of the tumor cavity plus a 1.5-cm margin, and the planning target volume was created by expanding the clinical target volume by 0.5 cm. LBRT was administered using a 6-MV linear accelerator to the tumor bed using a two-field technique according to a dose-fractionated schedule. Normally, LBRT was delivered at a total dose of 50 Gy in 25 fractions.

Statistical analysis

Postoperative differences in local recurrence, intracranial new metastases, the development of leptomeningeal metastases, and neurologic cause of death were compared between the WBRT and LBRT groups using the Fisher exact test. Numeric data, including RPA, KPS, and age, were compared using the Mann-Whitney *U* test. Progression-free survival was defined as the interval between the date of surgery to the date of the recognition of local recurrence or intracranial new metastases. Death was treated as an event, and the absence of disease progression was treated as a censored observation on the last day of follow-up. Overall survival was defined as the interval from the date of surgery to the date of death. Patients who were lost to follow-up were treated as a censored observation on the last day of follow-up. Univariate and multivariate analyses using the Cox proportional hazard model were performed to identify relevant factors affecting survival. The numeric factors analyzed in the Cox analyses were dichotomized according to the median number. All statistical analyses were performed using StatView, version 5.0 (SAS Institute, Tokyo, Japan).

RESULTS

Of the 421 surgical cases, we identified 130 patients who met the eligibility criteria. The characteristics of these patients are listed in Table 1. Of the 130 patients, 66 had received postoperative WBRT and 64 had received postoperative LBRT. Of the 66 patients who had received WBRT, 34 (51.5%) were treated to a dose of 30 Gy delivered in 10 fractions, and 31 (47.0%) were treated to a dose of 37.5 Gy delivered in 15 fractions. Of the 64 patients who received LBRT, 57 (89.1%) were treated to a dose of 50 Gy in 25 fractions, and 7 were treated with a variety of dose-fractionation schedules (24 Gy in 12 fractions to 60 Gy in 30 fractions).

The median progression-free survival period for the patients who received postoperative LBRT and WBRT was 9.7 and 11.5 months, respectively ($p = .75$; Fig. 1). The patients who underwent LBRT and WBRT developed 33 and 30 recurrences, respectively. The local recurrence rates (9.4% vs. 12.1%) and intracranial new metastases rates (42.2% vs. 33.3%) were not significantly different between the LBRT and WBRT groups (Table 2). The incidence of leptomeningeal metastases in patients receiving LBRT and WBRT was 9.4% and 10.6%, respectively ($p = .99$).

The median survival time for patients who received postoperative LBRT and WBRT was 13.9 and 16.7 months, respectively ($p = .88$; Fig. 2). Of the 64 patients who received LBRT and the 66 patients who received and WBRT, 59 and 49 died, respectively. A neurologic cause of death was noted in 35.6% of the patients in the LBRT group and 36.7% of the patients in the WBRT group ($p = .99$; Table 2). Univariate analyses revealed that only the RPA classification correlated significantly with survival (hazard ratio [HR], 0.436; $p = .002$). In particular, RT (LBRT vs. WBRT) did not correlate with survival (HR, 1.031; $p = .88$; Table 3). Multivariate analyses revealed that RPA was the only significant factor associated with survival (HR, 0.399; $p = .001$). Neither LBRT nor WBRT was related to survival (HR, 0.933; $p = .74$; Table 4).

Table 2. Patterns of treatment failure in patients who received WBRT and LBRT

Variable	LBRT ($n = 64$)	WBRT ($n = 66$)	
Total recurrences identified *(n)*	33	30	*p*
Local recurrence	6 (18.2)	8 (26.7)	.61
Distant metastasis	27 (81.8)	22 (73.3)	.61
Development of leptomeningeal metastases *(n)*	6	7	.99
Total deaths identified *(n)*	59	49	
Neurologic cause of death	21 (35.6)	18 (36.7)	.98*
Other	21 (35.6)	17 (34.7)	
Unknown	17 (28.8)	15 (30.6)	

Abbreviations: WBRT = whole brain radiotherapy; LBRT = local brain radiotherapy.
Data in parentheses are percentages.
* Chi-square test.

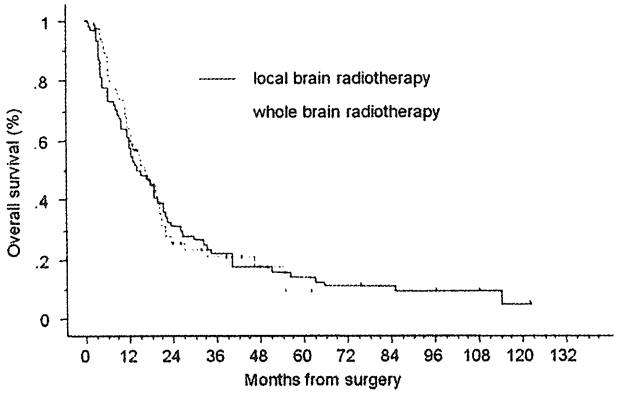

Fig. 2. Overall survival in patients with local brain radiotherapy (black line) and whole brain radiotherapy (dashed line).

We further analyzed the patterns of RT after recurrence in patients who received either postoperative LBRT or WBRT. Of the 33 patients who developed recurrences after postoperative LBRT, additional RT was performed in 15 (45.5%). Of the 15 patients, 6 underwent gamma knife or linear accelerator-based radiosurgery. LBRT was performed in 5 patients, and 4 received WBRT. Of the 30 patients who developed recurrences after postoperative WBRT, 16 (53.3%) received additional RT. Of the 16 patients, 13 received gamma knife or linear accelerator-based radiosurgery, and 3 received LBRT.

Among the patients who survived for >2 years, we compared the KPS at 2 years after surgery. A total of 20 patients who had received postoperative LBRT and 13 who had received postoperative WBRT were identified. The median KPS score at 2 years for these patients in the LBRT and WBRT groups was 80 (range, 60–100) and 80 (range, 60–100; $p = .99$), respectively. Of the 20 patients who had received LBRT, 9 experienced relapse in a local lesion, 2 had focal signs without relapse, which might have indicated radiation necrosis, and 7 had been well without relapse. For 2 other patients, this information was not available.

DISCUSSION

We have revealed the clinical outcomes of postoperative LBRT among patients with single metastasis and compared them with those of patients who underwent postoperative WBRT. The clinical outcomes, including progression-free survival, overall survival, local recurrence, intracranial new metastases, development of leptomeningeal metastases, and neurologic cause of death, were not significantly different between the two groups. In an analysis of relapse patterns, the patients treated with LBRT tended to have a lower probability of developing local recurrence (9.4% vs. 12.1%) and a greater probability of developing intracranial new metastases (42.2% vs. 33.3%), although these values were not significantly different. The probability of developing leptomeningeal metastases was also similar in each group (9.4% vs. 10.6%).

Previous reports have indicated that the addition of WBRT after tumor removal significantly reduces the local recurrence rate (3, 9). However, approximately 6–50% of patients develop relapses at new intracranial sites in the brain (5, 9, 19). Furthermore, about 20–30% of patients with brain metastasis die of neurologic causes even if a radiation boost has been added using stereotactic radiosurgery to increase local control, although the presence of extracranial lesions is the strongest factor for predicting survival (7, 20, 21). In our study, intracranial new metastases were predominant in both groups. The frequency of intracranial recurrence (new local and intracranial metastases) was somewhat greater than in previous series, although the rate of a neurologic cause of death was equivalent. Importantly, the patterns of treatment failure were similar in the LBRT and WBRT groups. Muacevic *et al.* (22) insisted that postoperative WBRT should be applied in patients with a single brain metastasis to destroy so-called micrometastases, based on the results of their randomized trial. They compared patients with a small single metastasis who received either surgery plus WBRT or gamma knife surgery alone. Their sample size was underpowered, although the risk of intracranial new metastases seemed to be lower in the WBRT cohort. To date, no randomized trials comparing the clinical outcomes of postoperative WBRT and postoperative gamma knife or linear accelerator-based radiosurgery, or LBRT have been reported.

We have demonstrated a similar efficacy for LBRT and WBRT. WBRT has problems in terms of delayed toxicity developing leukoencephalopathy, although the number of long-term survivors with brain metastasis seems to be somewhat low (11, 12). LBRT might be beneficial with regard to the protection of normal brain tissue. We compared the KPS

Table 3. Univariate analyses regarding survival

Variable	HR	95% CI	*p*
RT (LBRT vs. WBRT)	1.031	0.698–1.523	.88
RPA classification			
I vs. III	0.436	0.259–0.733	.002
II vs. III	0.808	0.514–0.127	.35
Removal status (gross total removal vs. partial removal)	0.948	0.385–2.334	.91
Tumor diameter (≥38 vs. <38 mm)	1.053	0.718–1.543	.79
Cancer type (lung cancer vs. other)	0.694	0.470–1.025	.062

Abbreviations: RT = radiotherapy; HR = hazard ratio; CI = confidence interval; other abbreviations as in Table 1.

Table 4. Multivariate analyses regarding survival

Variable	HR	95% CI	*p*
RT (LBRT vs. WBRT)	0.933	0.614–1.416	.743
RPA classification			
I vs. III	0.399	0.232–0.688	.001
II vs. III	0.736	0.455–1.191	.22
Removal status (gross total removal vs. partial removal)	0.622	0.239–1.615	.33
Tumor diameter (≥38 vs. <38 mm)	0.852	0.559–1.297	.45
Cancer type (lung cancer vs. other)	0.662	0.438–1.001	.05

Abbreviations as in Tables 1 and 3.

at 2 years to examine any delayed toxicity. Because of the nature of the present retrospective study, the detailed neurocognitive function or quality of life of the patients could not be identified. Among the long-term survivors, however, the KPS was preserved in both treatment groups. Thus, LBRT might be indicated for elderly patients at risk of developing dementia if LBRT has the same ability to control primary brain tumors, which is considered to be the main factor affecting neurocognitive function (14).

The present study had some limitations because of its retrospective nature. First, the radiation dose varied. About 90% of the LBRT patients received a dose of 50 Gy delivered in 25 fractions, and approximately 50% of the WBRT patients received a dose of 30 Gy delivered in 10 fractions; the others received a dose of 37.5 Gy delivered in 15 fractions. According to the summary by Tsao *et al.* (1), no differences in terms of survival or neurocognitive function were observed among the various dose-fraction schedules of WBRT. Second, the present study was a historical case-control study comparing LBRT and WBRT. Patients at risk of developing multiple metastases might have undergone WBRT during the period before 2004, when we started performing WBRT as the standard of care. Thus, the patients who were treated with LBRT might have had better general condition compared with the patients who were treated with WBRT. We compared the baseline characteristics of each treatment arm and used multivariate analyses to reduce any potential biases.

CONCLUSIONS

We have demonstrated the clinical efficacy of LBRT compared with WBRT on a large scale. The clinical outcomes, including progression-free survival, overall survival, patterns of treatment failure, development of leptomeningeal metastases, and a neurologic cause of death, were similar in both treatment groups. The KPS at 2 years was also similar when the two groups were compared. This result should be evaluated in a prospective manner.

REFERENCES

1. Tsao MN, Lloyd NS, Wong RK, *et al.* Radiotherapeutic management of brain metastases: A systematic review and meta-analysis. *Cancer Treat Rev* 2005;31:256–273.
2. Coia LR. The role of radiation therapy in the treatment of brain metastases. *Int J Radiat Oncol Biol Phys* 1992;23: 229–238.
3. Patchell RA, Tibbs PA, Regine WF, *et al.* Postoperative radiotherapy in the treatment of single metastases to the brain: A randomized trial. *JAMA* 1998;280:1485–1489.
4. Noordijk EM, Vecht CJ, Haaxma-Reiche H, *et al.* The choice of treatment of single brain metastasis should be based on extracranial tumor activity and age. *Int J Radiat Oncol Biol Phys* 1994;29:711–717.
5. Patchell RA, Tibbs PA, Walsh JW, *et al.* A randomized trial of surgery in the treatment of single metastases to the brain. *N Engl J Med* 1990;322:494–500.
6. Vecht CJ, Haaxma-Reiche H, Noordijk EM, *et al.* Treatment of single brain metastasis: Radiotherapy alone or combined with neurosurgery? *Ann Neurol* 1993;33:583–590.
7. Mintz AH, Kestle J, Rathbone MP, *et al.* A randomized trial to assess the efficacy of surgery in addition to radiotherapy in patients with a single cerebral metastasis. *Cancer* 1996;78:1470–1476.
8. Rades D, Fehlauer F, Schild S, *et al.* [Treatment for central neurocytoma: A meta-analysis based on the data of 358 patients]. *Strahlenther Onkol* 2003;179:213–218.
9. Nieder C, Astner ST, Grosu AL, *et al.* The role of postoperative radiotherapy after resection of a single brain metastasis: Combined analysis of 643 patients. *Strahlenther Onkol* 2007;183: 576–580.
10. Gaspar L, Scott C, Rotman M, *et al.* Recursive partitioning analysis (RPA) of prognostic factors in three Radiation Therapy Oncology Group (RTOG) brain metastases trials. *Int J Radiat Oncol Biol Phys* 1997;37:745–751.
11. Chao ST, Barnett GH, Liu SW, *et al.* Five-year survivors of brain metastases: A single-institution report of 32 patients. *Int J Radiat Oncol Biol Phys* 2006;66:801–809.
12. Lutterbach J, Bartelt S, Ostertag C. Long-term survival in patients with brain metastases. *J Cancer Res Clin Oncol* 2002; 128:417–425.
13. Sheline GE, Wara WM, Smith V. Therapeutic irradiation and brain injury. *Int J Radiat Oncol Biol Phys* 1980;6: 1215–1228.
14. Aoyama H, Tago M, Kato N, *et al.* Neurocognitive function of patients with brain metastasis who received either whole brain radiotherapy plus stereotactic radiosurgery or radiosurgery alone. *Int J Radiat Oncol Biol Phys* 2007;68:1388–1395.
15. Ueki K, Matsutani M, Nakamura O, *et al.* Comparison of whole brain radiation therapy and locally limited radiation therapy in the treatment of solitary brain metastases from non-small cell lung cancer. *Neurol Med Chir (Tokyo)* 1996;36:364–369.

16. Coucke PA, Zouhair A, Ozsahin M, *et al.* Focalized external radiotherapy for resected solitary brain metastasis: Does the dogma stand? *Radiother Oncol* 1998;47:99–101.
17. Iwadate Y, Namba H, Yamaura A. Whole-brain radiation therapy is not beneficial as an adjuvant therapy for brain metastases compared with localized irradiation. *Anticancer Res* 2002;22: 325–330.
18. Bahl G, White G, Alksne J, *et al.* Focal radiation therapy of brain metastases after complete surgical resection. *Med Oncol* 2006;23:317–324.
19. Smalley SR, Schray MF, Laws ER Jr., *et al.* Adjuvant radiation therapy after surgical resection of solitary brain metastasis: Association with pattern of failure and survival. *Int J Radiat Oncol Biol Phys* 1987;13:1611–1616.
20. Andrews DW, Scott CB, Sperduto PW, *et al.* Whole brain radiation therapy with or without stereotactic radiosurgery boost for patients with one to three brain metastases: Phase III results of the RTOG 9508 randomised trial. *Lancet* 2004;363:1665–1672.
21. Aoyama H, Shirato H, Tago M, *et al.* Stereotactic radiosurgery plus whole-brain radiation therapy vs stereotactic radiosurgery alone for treatment of brain metastases: A randomized controlled trial. *JAMA* 2006;295:2483–2491.
22. Muacevic A, Wowra B, Siefert A, *et al.* Microsurgery plus whole brain irradiation versus gamma knife surgery alone for treatment of single metastases to the brain: A randomized controlled multicentre phase III trial. *J Neurooncol* 2008;87:299–307.

No Shinkei Geka, 39(10): 991 - 997, 2011

症例 ◆ Case Report

胆管細胞癌よりの脈絡叢転移性腫瘍の1例*

栗栖 宏多[1], 鴨嶋 雄大[1], 寺坂 俊介[1], 小林 浩之[1], 久保田 佳奈子[2], 寶金 清博[1]

A Case of Metastatic Choroid Plexus Tumor from Cholangiocellular Carcinoma

Kota KURISU[1], Yuuta KAMOSHIMA[1], Shunsuke TERASAKA[1], Hiroyuki KOBAYASHI[1], Kanako KUBOTA[2], and Kiyohiro HOUKIN[1]

Key words:
metastatic tumor, intraventricular tumor, choroid plexus, Ber EP-4, cholangiocellular carcinoma

Metastatic intraventricular tumor located in the choroid plexus is very rare. Only a few cases have been reported in the past. According to past reports, these tumors originated from lung, colon, and so on, but not from the bile duct. This is the first case report of choroid plexus metastasis from cholangiocellular carcinoma.

A 57-year-old woman who had a history of cholagiocellular carcinoma, demonstrated intraventricular tumor. Although sufficient examination was performed, the tumor was difficult to diagnose as being a metastatic tumor or a choroid plexus carcinoma. Because of this, we performed endoscopic biopsy of the intraventricular tumor. However intraoperative findings were not helpful in distinguishing metastatic tumor and choroid plexus carcinoma. Postoperatively, histological examination was performed. However it was still difficult to differentiate this rare tumor from choroid plexus carcinoma by only hematoxylin and eosin stain. For further examination, Ber EP-4 stain was performed. Ber EP-4 showed strongly positive which indicates metastatic tumor. This method led us to make an appropriate diagnosis of this extremely rare tumor.

We considered that in order to diagnose this rare tumor, appropriate histopathological examination, including immunohistopathological examination should be performed.

(Received : March 10, 2011, Accepted : April 25, 2011)

No Shinkei Geka 39(10): 991 - 997, 2011

I. はじめに

脈絡叢乳頭腫や脈絡叢乳頭癌は比較的稀な脳腫瘍である．その発生頻度は人口10万人当たり0.3人に発生するといわれ[9,10]，全脳腫瘍のうち0.4～0.8%[30]を占めるに過ぎない．一方で，頭蓋外原発の悪性腫瘍の脈絡叢転移も極めて稀である．われわれが渉猟し得た限りでは，過去に35例の報告[3,7,13,20,23-26,28,29]しかない．この35例のうち，原発巣としては腎癌の報告[23-26]が最も多く，次いで肺・大腸[7,24]と続いている．しかし，胆管細胞癌からの転移は過去に報告例はない．両者の鑑別はその稀少性ゆえに時として臨床所見（画像所見），病理所見において困難を伴う．

*(2011. 3. 10受稿，2011. 4. 25受理)

1）北海道大学病院脳神経外科，Department of Neurosurgery, Hokkaido University Hospital
2）同 病理部，Department of Pathology, Hokkaido University Hospital
〔連絡先〕栗栖宏多＝北海道大学病院脳神経外科（〒060-8648 札幌市北区北14条西5丁目）
Corresponding author : Kota KURISU, M.D., Department Neurosurgery, Hokkaido University Hospital, North-14 West-5, Kitaku, Sapporo-city, Hokkaido 060-8648, JAPAN

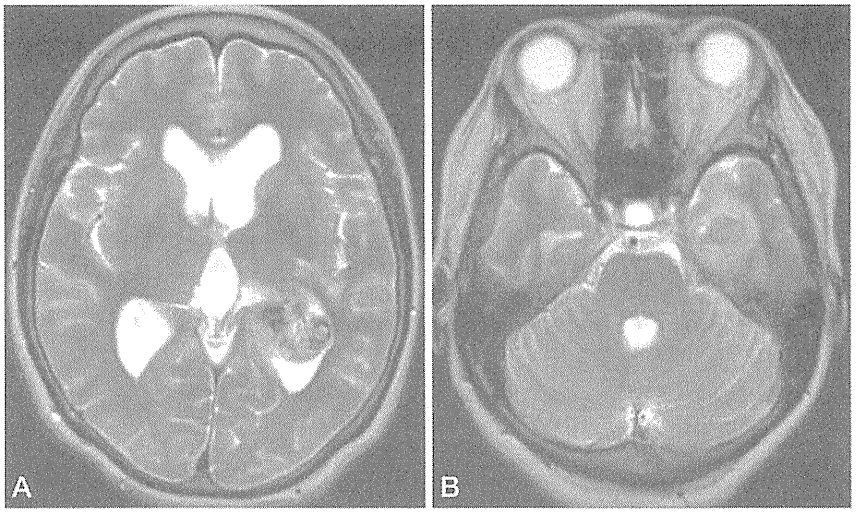

Fig. 1 T2 weighted imaging on admission. A: Intraventricular tumor in the left trigone demonstrated mixed intensity. And the tumor was accompanied with peritumoral edema. B: The tumor located in the left inferior horn was observed.

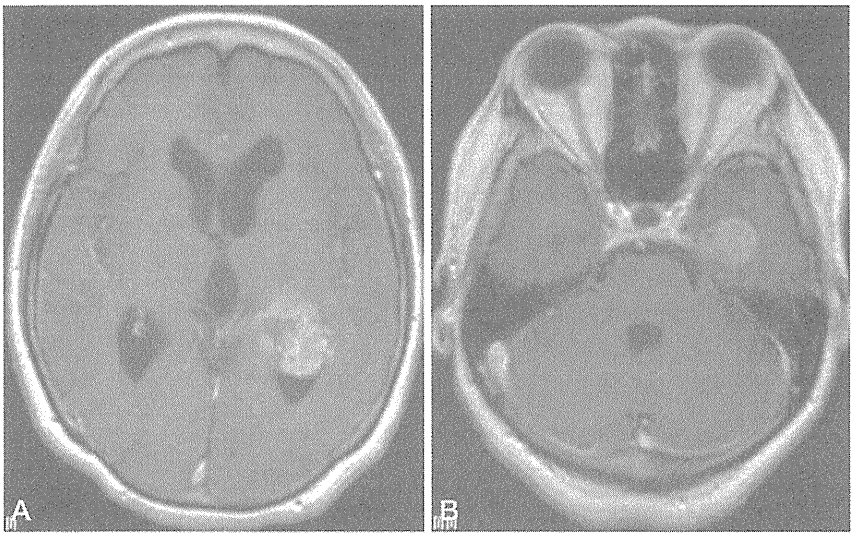

Fig. 2 T1 weighted image after administration of gadolinium. A: The tumor was strongly enhanced. B: The tumor located in the left inferior horn was also strongly enhanced.

今回，われわれは成人担癌患者（胆管細胞癌）に側脳室内脈絡叢部に腫瘍が認められた症例を経験した．画像所見，病理所見を含め原発性腫瘍，転移性腫瘍の鑑別が問題となったが，病理組織診断を用いて最終診断として転移性腫瘍との診断に至った．この非常に稀であり，診断に難渋した症例をその診断過程も含めて若干の文献的考察を加えて報告する．

II．症　例

〈患　者〉 57歳　女性

現病歴　2010年6月に前医外科にて肝内胆管細胞癌に対する根治術を施行された．前医での病

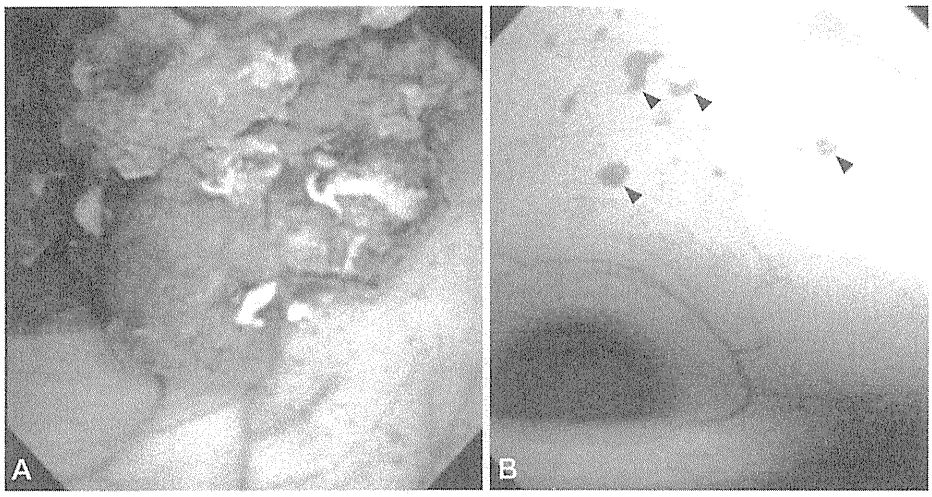

Fig. 3 Intraoperative photographs. A: The intraventricular tumor was reddish and soft, partly calcified and highly vascular and originated from the choroid plexus. B: In the 3rd ventricle, disseminated lesions (**arrow heads**) were observed.

理組織診断にて胆管細胞癌（tubular adenocarcinoma）で脈管侵襲はなく，断端陰性と診断された．術後明らかな再発や転移は指摘されず，外来経過観察中であった．

2010年9月，偶発的に前医脳神経外科で施行された頭部magnetic resonance imaging（MRI）にて，側脳室内腫瘍性病変が指摘され，当科に紹介となった．

神経学的陽性所見　特記事項なし

血液生化学的評価　各種腫瘍マーカーはalpha fetoprotein（AFP）：3.1 ng/mL（基準値1.0～10.0 ng/mL），carcinoembryonic antigen（CEA）：3.1 ng/mL（基準値1.0～6.5 ng/mL），carbohydrate antigen 19-9（CA19-9）：63.0 U/mL（基準値0～37 U/mL），suquamous cell carcinoma（SCC）抗原：0.7 ng/mL（基準値0～1.5 ng/mL）とCA 19-9の高値を認めた．また髄液細胞診断からは異常形態を示す細胞は検出されなかった．

画像評価　当院にて撮像を行った頭部computed tomography（CT）では，左側脳室内三角部に石灰化を伴った腫瘍性病変を認め，同様に同側下角先端部にも石灰化を伴った腫瘍性病変が認められた．MRIではこれらの腫瘍性病変は不整形で脳実質とほぼ等信号を示し，腫瘍内部にはT2強調画像（**Fig. 1**）で低信号領域が散在していた．同腫瘍は隣接脳実質に浸潤傾向を示し，gadolinium造影像では腫瘍は不均一で著明な増強効果を伴っていた（**Fig. 2**）．このほか第四脳室Luschka孔部にも病変の存在が疑われた．全脊髄MRIも施行されたが明らかな腫瘍病変は認めなかった．

以上より，左側脳室三角部に発生した転移性脈絡叢腫瘍もしくは脈絡叢乳頭癌の頭蓋内播種性病変と考え，腫瘍病変の全身検索を目的としてFDG-PETを含めた各種画像評価を行ったが，頭蓋内以外に腫瘍病変を認めなかった．頭蓋内腫瘍病変は全摘出が困難であることから，原発性病変，転移性病変の両者を考慮した，全脳全脊髄照射を本段階で行うことも検討したが，患者側からの病理組織診断への強い希望もあり，2010年10月，内視鏡下脳室内腫瘍生検術を実施した．術中所見では易出血性，脆弱な腫瘍性病変を脳室三角部脈絡叢に認め，同時に側脳室，第三脳室内に播種性病変を認めた（**Fig. 3**）．同脈絡叢部の腫瘍の病理組織診断を行った．

病理組織所見　病理学的には腫瘍はhematoxylin-eosin（H.E.）染色で異型の強い核を有する細胞が乳頭状増生を示し，脈絡叢乳頭癌として矛盾しない所見であったが（**Fig. 4**），後日追加で行っ

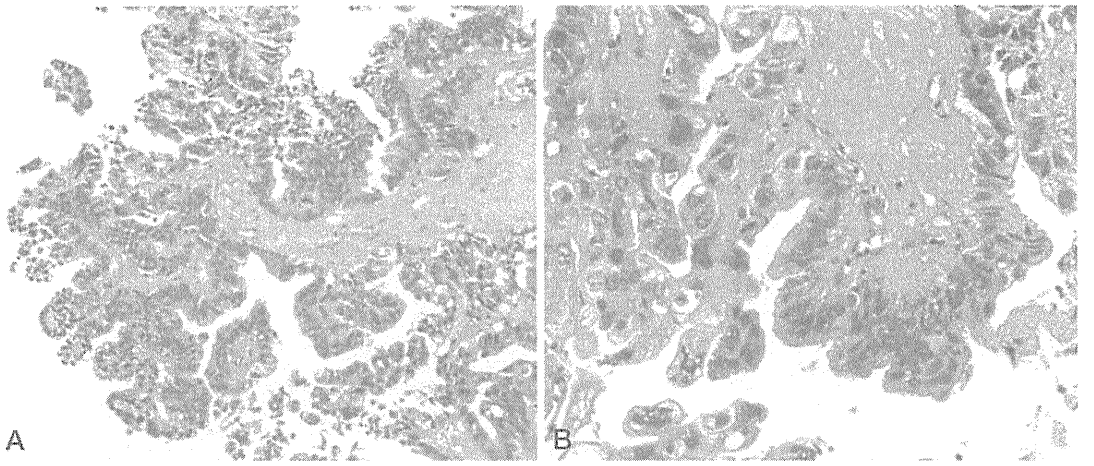

Fig. 4 Histopathological photographs (hematoxylin and eosin stain). A: low magnification, B: high magnification. Tumor with a papillary configuration was observed, and a pleomorphic nucleus was also observed.

た免疫染色にて glial fibrillary acidic protein(GFAP)陰性，transthyretin 陰性，S100 protein 陰性であり，脈絡叢乳頭癌としては非典型的であり，Ber-EP4 の免疫染色を追加したところ正常脈絡叢との境界が明瞭な陽性を示し，最終的に胆管細胞癌の脈絡叢転移と診断した（**Fig. 5**）．患者は確定診断後，放射線治療により全脳全脊髄照射(30.6 Gy＋boost 14.4 Gy）を行い，現在は経過観察中である．

Ⅲ. 考　察

脳室内腫瘍の発生頻度は比較的稀であり，その診断には難渋することが多い．今回，われわれは術前には確定診断に至らず，生検術を行い，過去に報告例のない胆管細胞癌の脈絡叢転移と診断できた 1 例を経験した．

胆管細胞癌は比較的稀な消化器悪性腫瘍であり[12,16]，その発生頻度は 10 万人当たり 1 ～ 2 人に発症する[22]といわれ，胃腸器系に発生する癌の 3%[27]を占める．一般に転移性脳腫瘍は癌治療の進歩，癌年齢人口の増加に伴いその頻度が増加しており，Kaal ら[11]は担癌患者の 25%に認めると報告している．しかし脈絡叢転移は比較的稀であり，その頻度は，頭蓋外悪性腫瘍にて死亡した 737 例の剖検例の検討によっても 2.6%にしか認められないという報告[21]がある．さらに Al-Anazi ら[1]と Kohno ら[15]によると，脳室内腫瘍そのものの頻度が低い中で転移性腫瘍は 6%に過ぎず，また頭蓋内転移性腫瘍のうち脈絡叢転移は 0.14%と極めて稀である．脈絡叢の転移性腫瘍の報告は渉猟し得るもので過去 35 例[3,7,13,20,23-26,28,29]を認めるのみであり，自験例を加えても 36 例に過ぎない．この中で，臓器別の腫瘍原発巣は，多い順より腎臓 16 例（44.4%）[23-26]，肺 4 例（11.1%）[7,24]，大腸 4 例（11.1%）[24]，甲状腺 3 例（8.3%）[3,28,29]の報告を認めた．しかしながら本症例のように胆管細胞癌の脳室内，脈絡叢転移の報告は認めず，本報告が初めてのものとなる．この稀少性から，本症例では術前の臨床所見や画像所見から診断に至らず，病理組織診断においても確定診断に難渋した．

一般に側脳室内腫瘍を認めた場合，髄膜腫や上衣腫，悪性リンパ腫などさまざまな原発性腫瘍性病変が鑑別疾患として挙げられるが，本症例においては転移性脈絡叢腫瘍と脈絡叢乳頭癌の鑑別が問題となった．本症例で患者は，受診時に胆管細胞癌の既往は既知の情報であったが，FDG-PET を含めた各種全身検索では脳室内腫瘍以外に明らかな腫瘍性病変は認めなかった．一方，胆管細胞癌の腫瘍マーカーとして汎用されている血清 CA19-9 は異常高値を示しており，胆管細胞癌の再発もしくは転移性腫瘍の存在を示唆する所見であった[12,16]が，胆管細胞癌の術後であること，ま

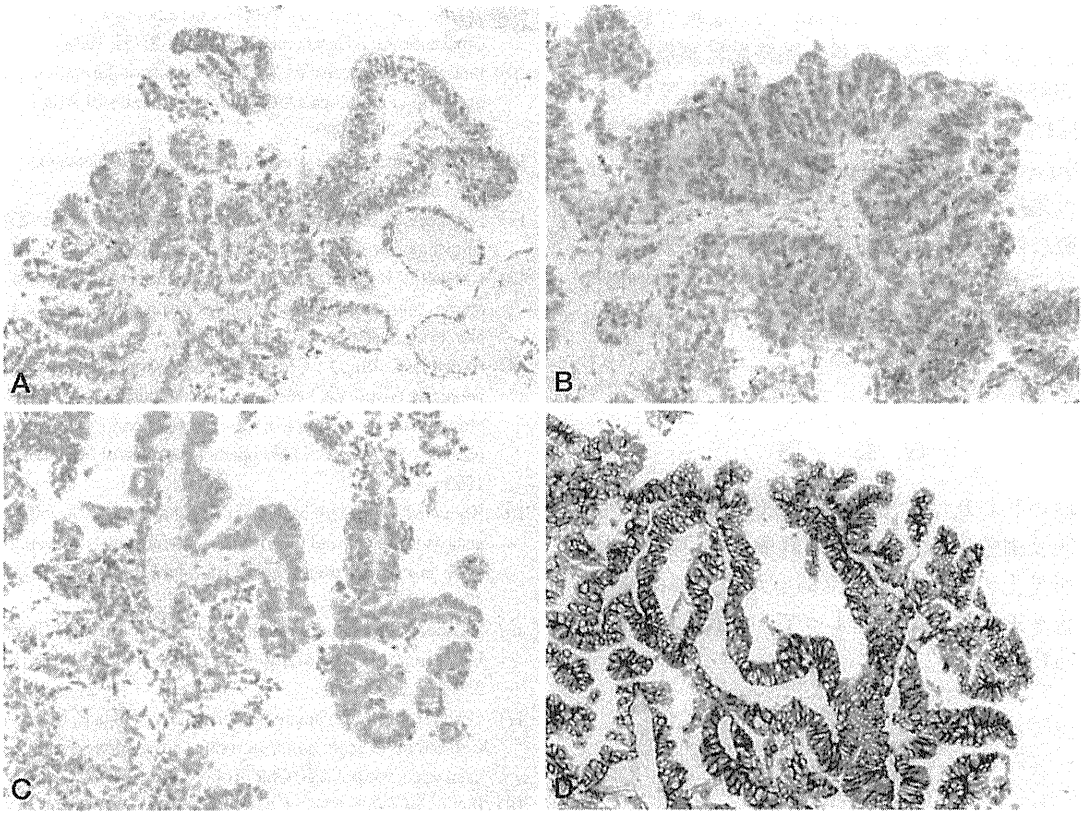

Fig. 5 Immunohistochemical examination. A: GFAP, B: S100 protein, C: transthyretine, D: Ber EP-4

た脈絡叢乳頭癌でも高値を示すとする報告[8,17]もあり，両者の鑑別における決定的な所見とはいえなかった．画像所見上も左側脳室内後角に分葉状の強い増強効果を示す病変があり，さらに下角先端部や第四脳室左側 Luschka 孔に沿った多発性の病変を認め，隣接脳実質への浸潤性の変化も認めており，脈絡叢の転移性腫瘍，もしくは脈絡叢乳頭癌どちらにおいても矛盾しない所見であった．このため両者を病理組織診断なしに鑑別することは困難であった．

さらに本症例の病理組織診断では，H.E. 染色標本上も組織像として脈絡叢乳頭癌としても矛盾しない所見が得られており，病理医においても転移性腫瘍と脈絡叢乳頭癌の鑑別に時間を要した．診断に際して脈絡叢乳頭癌の免疫染色法には多数の報告があるが，感度・特異度の高いものに関してはまだ議論の余地がある[2,4,18,19]．その一方で脈絡叢原発性腫瘍と転移性腫瘍との病理学的な鑑別に関しては，いくつかの免疫染色法の報告があり[5,6,14]，Kepes ら[14]は synaptophysin による免疫染色がこの鑑別に有効とも報告しているが，本症例では行わなかった．また，Gyure ら[6]は cytokeratin（CK）7 と CK20 を用いた脈絡叢原発性腫瘍と転移性脈絡叢腫瘍の鑑別について報告している．しかし本症例では，既往としてあった胆管細胞癌の CK7/CK20 のフェノタイプは，脈絡叢原発性腫瘍の大半（74％）を示す CK7 positive/CK20 negative と一致しており，鑑別に有用でなかった．このほかにも腫瘍マーカーである CEA[18]や CA19-9[17]の免疫染色が鑑別に有用であるという報告があるが，これは脈絡叢原発性腫瘍の診断に CEA や CA19-9 の免疫染色が有用であったという報告であり，胆管細胞癌の既往がある本症例では有効ではなかった．Gottschalk ら[5]は上皮性抗原である

HEA125 と Ber EP-4 は，非常に高い感度で脈絡叢原発性腫瘍（脈絡叢乳頭腫，脈絡叢乳頭癌）と脈絡叢の転移性腫瘍を鑑別できると報告している．本症例では，各種免疫染色にて GFAP 陰性，transthyretin 陰性，S100 protein 陰性であり，Ber-EP4 の免疫染色を追加したところ正常脈絡叢と境界明瞭に陽性を示し，胆管細胞癌の脈絡叢転移との診断に至っており，同免疫染色法の高い有用性が認められた．今後，自験例のようなケースにおいて考慮すべき染色法である．

IV. 結　語

今回われわれは，側脳室内脈絡叢に認められた稀な胆管細胞癌転移性腫瘍を経験した．画像所見，病理所見上の診断は困難であったが，Ber-EP4 免疫染色を追加することによって，最終診断が可能であった．

文　献

1) Al-Anazi A, Shannon P, Guha A：Solitary metastasis to the choroid plexus. Case illustration. J Neurosurg **92**：506, 2000
2) Coffin CM, Wick MR, Braun JT, Dehner LP：Choroid plexus neoplasms. Clinicopathologic and immunohistichemical studies. Am J Surg Pathol **10**：394-404, 1986
3) Ferrer Garcia JC, Merino Torres JF, Ponce Marco JL, Pinon Selles F：Unusual metastasis of differentiated thyroid carcinoma [In Spanish]. An Med Interna **19**：579-582, 2002
4) Gopal P, Parker JR, Debski R, Parker JC：Choroid plexus carcinoma. Arch Pathol Lab Med **132**：1350-1354, 2008
5) Gottschalk J, Jautzke G, Paulus W, Goebel S, Cervos-Navarro J：The use of immunomorphology to differentiate choroid plexus tumors from metastatic carcinomas. Cancer **72**：1343-1349, 1993
6) Gyure KA, Morrison A：Cytokeratin 7 and 20 expression in choroid plezus tumors：Utility in differentiating these neoplasms from metastatic carcinoma. Mod Pathol **13**：638-643, 2000
7) Healy JF, Rosenkrantz H：Intraventricular metastasis demonstrated by cranial computed tomography. Radiology **136**：124, 1980
8) Inamura T, Nishio S, Miyagi Y, Kamikaseda K, Ueda K, Fukui M, Yoshimoto K：Primary choroid plexus carcinoma producing carbohydrate antigen 19-9. Clin Neuropathol **19**：268-272, 2000
9) Janisch W, Staneczek W：Epidemiology of tumors of the central nervous system – influence of the autopsy rate on the incidence rate. Arch Geschwulstforsch **58**：51-55, 1988
10) Janisch W, Staneczek W：Primary tumors of the choroid plexus：Frequency, localization and age. Zentralbl Allg Pathol **135**：235-240, 1989
11) Kaal EC, Niel CGJH, Vecht CJ：Therapeutic management of brain metastasis. Lancet Neurol **4**：289-298, 2005
12) Kahn SA, Thomas HC, Davidson BR, Taylor-Robinson SD：Cholangiocarcinoma. Lancet **366**：1303-1314, 2005
13) Kendall B, Reider-Grosswasser I, Valentine A：Diagnosis of masses presenting within the ventricles on computed tomography. Neuroradiology **25**：11-22, 1983
14) Kepes JJ, Collins J：Choroid plexus epithelium (normal and neoplastic) expresses synaptophysin. A potentially useful aid in differentiating carcinoma of the choroid plexus from metastatic papillary carcinomas. J Neuropathol Exp Neurol **58**：398-401, 1999
15) Kohno M, Matsutani M, Sasaki T, Takakura K：Solitary metastasis to the choroid plexus of the lateral ventricle：report of three cases and a review of the literature. J Neurooncol **27**：47-52, 1996
16) Mosconi S, Bretta GD, Labianca R, Zampino MG, Gatta G, Heinemann V：Cholangiocarcinoma. Hematology **69**：259-270, 2009
17) Osada H, Mori K, Yamamoto T, Nakao Y, Wada R, Maeda M：Choroid plexus carcinoma secreting carbohydrate antigen 19-9 in an adult. Neurol Med Chir (Tokyo) **46**：251-253, 2006
18) Paulus W, Janisch W：Clinicopathologic correlations in epithelial choroid plexus neoplasms：a study of 52 cases. Acta Neuropathol **80**：635-641, 1990
19) Paulus W, Brandner S：Synaptophysin in choroid plexus epithelial cells：no useful aid in differential diagnosis. J Neuropathol Exp Neurol **58**：1111-1112, 1999
20) Puppa AD, Pos SD, Zovato S, Orvieto E, Ciccarino P, Manara R, Zustovich F, Berti F, Gardiman MP, Scienza R：Solitary intra-ventricular brain metastasis from a breast carcinoma. J Neurooncol **97**：123-126, 2010
21) Schreiber D, Bernstein K, Schneider J：Metastases of the central nervous system. A third communication. Metastases in the pituitary gland, pineal gland, and choroid plexus. Zentralbl Allg pathol **126**：64-73, 1982
22) Shaib YH, El-Serag HB, Davila JA, Morgan R, McGlynn KA：Risk factors of intrahepatic cholangiocarcinoma in the United States：a case-control study. Gastroenterology **128**：620-626, 2005
23) Spetzger U, Mull M, Sure U, Gilsbach J：Subarachnoid and intraventricular hemorrhage caused by hypernephroma metastasis, accompanied by innocent bilateral posterior communicating artery aneurysms. Surg Neurol **44**：275-278, 1995
24) Sung WS, Dubey A, Erasmus A, Hunn A：Solitary choroid plexus metastasis from carcinoma of the oesophagus. J Clin Neurosci **15**：594-597, 2008
25) Tomiyama A, Nakayama H, Aoki K, Ueda M：Solitary metastasis of renal cell carcinoma to the third ventricular choroid

plexus with rapid clinical manifestation by intratumoral hemorrhage. Neurol India **56**：179-181, 2008
26) Toms SA, Suh JH, Weil RJ. Choroid plexus metastasis：Urology **70**：370-371, 2007
27) Vauthey JN, Blumgart LH：Recent advances in the management of cholangiocarcinomas. Semin Liver Dis **14**：109-114, 1994
28) Wasita B, Sakamoto M, Mizushima M, Kurosaki M, Watanabe T：Choroid plexus metastasis from papillary thyroid carcinoma presenting with intraventricular hemorrhage：case report. Neurosurgery **66**：E1213-E1214, 2010
29) Zhang YA, Kavar B, Drummond KJ：Thyroid carcinoma metastasis to the choroid plexus of the lateral ventricle. J Clin Neurosci **16**：118-121, 2009
30) Zulch KJ：Brain tumors, there biology and pathology 1st edition. Springer-Verlag, New York, 1957

A feasibility study of a molecular-based patient setup verification method using a parallel-plane PET system

2011 Phys. Med. Biol. 56 965

(http://iopscience.iop.org/0031-9155/56/4/006)

IOP PUBLISHING PHYSICS IN MEDICINE AND BIOLOGY

Phys. Med. Biol. 56 (2011) 965–977 doi:10.1088/0031-9155/56/4/006

A feasibility study of a molecular-based patient setup verification method using a parallel-plane PET system

Satoshi Yamaguchi[1], Masayori Ishikawa[1], Gerard Bengua[2], Kenneth Sutherland[1], Teiji Nishio[3], Satoshi Tanabe[1], Naoki Miyamoto[1], Ryusuke Suzuki[2] and Hiroki Shirato[4]

[1] Department of Medical Physics and Engineering, Hokkaido University Graduate School of Medicine, N-15 W-7 Kita-ku Sapporo 060-8638, Japan
[2] Department of Medical Physics, Hokkaido University Hospital, N-14 W-5 Kita-ku Sapporo 060-8648, Japan
[3] Particle Therapy Division, Research Center for Innovative Oncology, National Cancer Center, Kashiwa, 6-5-1 Kashiwano-ha, Kashiwa-shi, Chiba 277-8577, Japan
[4] Department of Radiology, Hokkaido University Graduate School of Medicine, N-15 W-7 Kita-ku Sapporo, 060-8638 Japan

E-mail: masayori@med.hokudai.ac.jp

Received 15 July 2010, in final form 9 December 2010
Published 19 January 2011
Online at stacks.iop.org/PMB/56/965

Abstract

A feasibility study of a novel PET-based molecular image guided radiation therapy (m-IGRT) system was conducted by comparing PET-based digitally reconstructed planar image (PDRI) registration with radiographic registration. We selected a pair of opposing parallel-plane PET systems for the practical implementation of this system. Planar images along the in-plane and cross-plane directions were reconstructed from the parallel-plane PET data. The in-plane and cross-plane FWHM of the profile of 2 mm diameter sources was approximately 1.8 and 8.1 mm, respectively. Therefore, only the reconstructed in-plane image from the parallel-plane PET data was used in the PDRI registration. In the image registration, five different sizes of ^{18}F cylindrical sources (diameter: 8, 12, 16, 24, 32 mm) were used to determine setup errors. The data acquisition times were 1, 3 and 5 min. Image registration was performed by five observers to determine the setup errors from PDRI registration and radiographic registration. The majority of the mean registration errors obtained from the PDRI registration were not significantly different from those obtained from the radiographic registration. Acquisition time did not appear to result in significant differences in the mean registration error. The mean registration error for the PDRI registration was found to be 0.93 ± 0.33 mm. This is not statistically different from the radiographic registration which had a mean registration error of 0.92 ± 0.27 mm. Our results suggest

0031-9155/11/040965+13$33.00

that m-IGRT image registration using PET-based reconstructed planar images along the in-plane direction is feasible for clinical use if PDRI registration is performed at two orthogonal gantry angles.

(Some figures in this article are in colour only in the electronic version)

1. Introduction

Image guided radiotherapy (IGRT) techniques are presently used clinically to improve the accuracy of treatment delivery in photon radiation therapy. IGRT is used to correct for patient positioning errors prior to or during treatment by using image guided procedures. Patient setup can be verified through the co-registration of digitally reconstructed radiographs (DRR) and imaging plate (IP) or electronic portal imaging device (EPID) images taken using MV-x rays from a linear accelerator (Linac) while the patient is set up just prior to treatment (Dong and Boyer 1995, Gilhuijs *et al* 1996). Linac systems with on-board cone-beam computed tomography (CBCT) devices have also been developed (Pouliot *et al* 2005, Jaffray *et al* 2002, Groh *et al* 2002, Ford *et al* 2002, Munbodh *et al* 2006). CBCT allows the imaging of the target volume and organs at risk during treatment. Accuracy of patient setup verification error is important in order to ensure that the actual treatment geometry is as close as possible to the treatment planning geometry. At present, patient setup verification is done mostly by the alignment of bony structures in radiographic images taken during treatment and those used for treatment planning. The change in the tumor size and location inside the body is usually difficult to determine during treatment. Making the tumor visible in the irradiation field is thus desirable in order to improve setup verification accuracy.

Positron emission tomography (PET) based on sugar metabolism in the tumor caused by ^{18}F-fluorodeoxyglucose (FDG) uptake has been shown to be effective for distinguishing the tumor during diagnosis (Som *et al* 1980). Since PET images are functional images, they allow cell activity to be visible; thus, the tumor position can be determined. Another promising radioactive tracer for PET imaging is ^{18}F-fluoromisonidazole (FMISO) (Nehmeh *et al* 2008). FMISO is able to delineate hypoxic cells, which are known to be radiation resistant, in tumors. Clinical trials have demonstrated improved tumor control by delivering escalated doses to hypoxic tumor cells using IMRT and other techniques (Lee and Le 2008).

The spatial resolution and sensitivity of recent PET devices have also been significantly improved. This has been partly due to (1) the development of new detector elements such as BGO or GSO crystals, (2) the change in the acquisition method from 2D to 3D, and (3) the invention of depth-of-interaction (DOI) (Wienhard *et al* 2002, Yamaya *et al* 2003). The application of PET technology as a new modality for diagnostic procedures is also now being considered, for example, positron emission mammography (PEM) (Smith *et al* 2003, Huesman *et al* 2000, Zhang *et al* 2007, Raylman *et al* 2008, MacDonald *et al* 2009). In this study, we propose a PET-based molecular image guided radiation therapy (m-IGRT) system for patient setup verification in cases where significant tumor shrinkage or growth may occur, such as intracranial or head and neck. In the practical implementation of an m-IGRT system, it is preferable that the PET device is combined with a radiotherapy gantry to guarantee mechanical precision. There are, however, some restrictions on how the PET detectors can be mounted to the present gantry systems.

Because PET is a device that detects the annihilation radiation caused by positrons, it is necessary that at least a pair of opposed detectors are arranged to detect the two photons simultaneously. It is preferable that the isocenter of the pair of opposed detectors is identical to the isocenter of the radiotherapy unit. A structure with a wide open space between a pair of

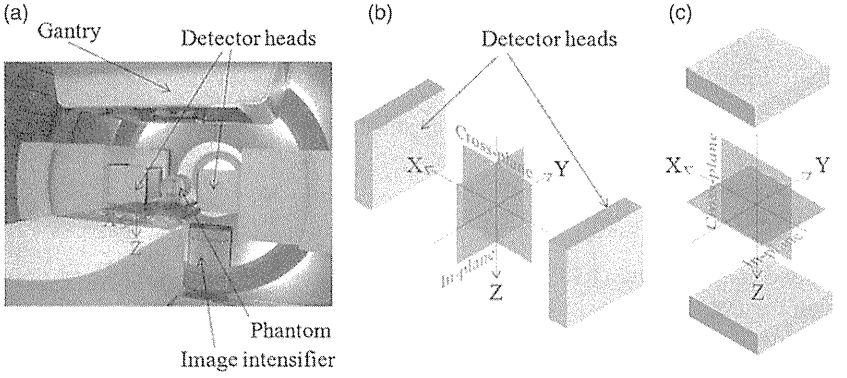

Figure 1. (a) The BOLPs with its gantry positioned at 0°. (b) The orientations of the in-plane and cross-plane directions in the BOLPs at a gantry angle of 0°. (c) The orientations of the in-plane and cross-plane directions in the BOLPs at a gantry angle of 90°.

opposed detectors is also needed so that the mega-voltage irradiation field does not become obstructed. The gantry rotation of the radiotherapy unit and the movement or the rotation of the couch must also be considered. Moreover, it is necessary to secure a wide field of view to use the device for setup verification. However, it is difficult in the conventional PET detector geometry, with ring-shape arrangement, to achieve this purpose. We therefore selected a geometry with a pair of opposing parallel-plane detectors. The advantage of this detector geometry is that it is structurally simple, and that it can be mounted easily on a radiotherapy gantry, similar to on-board imaging (OBI) devices.

In order to evaluate the feasibility of molecular image guided registration, we used the beam on-line PET system (BOLPs), developed at the Particle Therapy Division of the National Cancer Center, Kashiwa (Nishio *et al* 2005, 2006, 2010). The system consists of a pair of opposing parallel-plane detectors mounted on the gantry which can detect annihilation radiation produced by positron emitters (e.g. ^{15}O, ^{14}O, ^{13}N and ^{11}C). The BOLPs was originally developed for visualizing irradiation fields by measuring the activity of positron emitters which are generated by nuclear reactions from incident proton beams. The BOLPs has the same detector configuration as that of our proposed system.

In this paper, we report on the feasibility of a novel m-IGRT by comparing the PET-based digitally reconstructed planar image (PDRI) registration with radiographic registration.

2. Materials and method

2.1. Beam on-line PET system

The BOLPs at the National Cancer Center, Kashiwa, in Japan was used to verify the accuracy of patient setup verification in our proposed parallel-plane PET system. The BOLPs detector is mounted at the gantry of the proton irradiation system as shown in figure 1(a). The detector head consists of 3960 BGO crystals (2 mm × 2 mm × 20 mm) covering a 16 × 16 cm^2 field of view. The distance between the detector heads was fixed at 40 cm. Shown in figure 1(b) are the orientations of the in-plane and cross-plane directions for a gantry angle of 0°. The orientations of the in-plane and cross-plane directions for a gantry angle of 90° are illustrated in figure 1(c). The evaluation of the full width at half maximum (FWHM) of the profile of

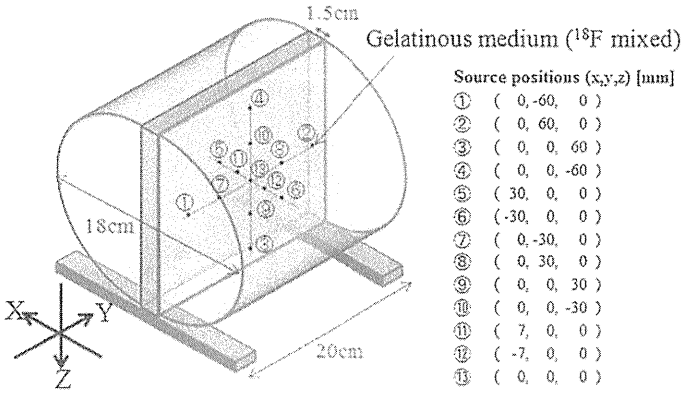

Figure 2. Cylindrical phantom with ^{18}F-sources placed in the positions as indicated.

2 mm diameter sources was done along the cross-plane and in-plane directions for a gantry angle of 0°. The FWHM of the profile is indicative of the spatial resolution.

In the image registration, only the reconstructed in-plane image from the parallel-plane PET data was used, and from here on, this in-plane image will be referred to as PDRI.

The BOLPs also includes an on-board x-ray system that allows the acquisition of radiographic images for patient setup verification. We compared the accuracy of radiographic and PDRI registrations.

2.2. *Image reconstruction method*

The detector configuration of the BOLPs is different from that of conventional PET systems in that they do not encircle the subject. Due to the parallel placement of the detector heads, there is limited angular sampling and loss of line of response (LOR) and the usual sinogram-based reconstruction method is not applicable. Therefore, the maximum likelihood-expectation maximization (MLEM) method (Shepp and Vardi 1982) was used in the LOR-based reconstruction using Siddon's algorithm (Siddon 1985).

In this study, only the detector sensitivity correction was applied while ignoring the other possible correction factors to account for scattering or absorption.

2.3. *Phantom configuration*

Two custom-made phantoms were used in our measurements. The first phantom was a polycarbonate cylindrical phantom with a width of 20 cm and a diameter of 18 cm. We refer to this phantom as the *cylindrical phantom*. It contained 13 cylindrical radiation sources (each with a diameter of 2 mm and width of 2 mm) that were arranged as shown in figure 2. The other phantom was a polycarbonate plate containing five cylindrical radiation sources of various diameters (i.e. 8, 12, 16, 24, 32 mm) with 1.5 cm width, representing different tumor sizes as shown in figure 3(a). This was attached to an acrylic slab (height: 20 cm, width: 18.5 cm, depth: 0.3 cm) as shown in figure 3(b). In this paper, we refer to this phantom setup as the *tumor phantom*. The radiation sources in both the cylindrical phantom and the tumor phantom used ^{18}F that was homogeneously mixed in a gelatinous medium.

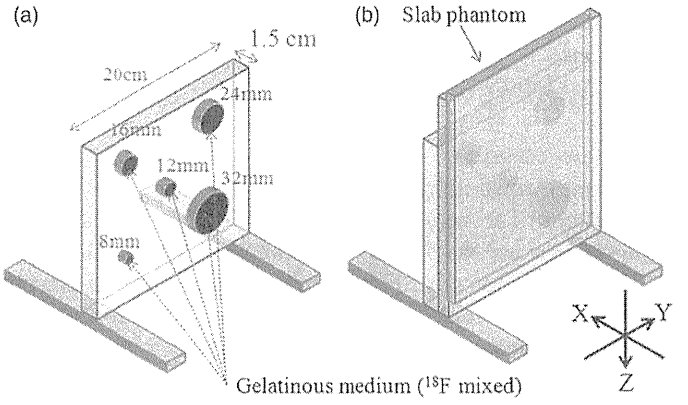

Figure 3. (a) Polycarbonate plate containing ^{18}F-sources of various diameters representing different tumor sizes. (b) The plate in (a) attached to an acrylic slab phantom.

2.4. FWHM of the profile of 2 mm diameter sources

The unique detector geometry of the BOLPs does not allow the use of the filtered back projection reconstruction as specified in the National Electrical Manufactures Association (NEMA) standard which is used for the evaluation of PET detectors. Therefore we used a modified method for image reconstruction based on PEM (Smith *et al* 2004, MacDonald *et al* 2009), which has a detector geometry similar to the BOLPs. PEM devices and the BOLPs have anisotropic spatial resolutions because the detectors do not encircle the object and do not rotate to acquire the full 360° angular sampling required for full three-dimensional tomography. Parallax error caused by the thickness of scintillation crystals is considered (Hoffman *et al* 1989, Lerche *et al* 2005).

We evaluated the FWHM of the profile of 13 cylindrical sources with a diameter of 2 mm and width of 2 mm using the cylindrical phantom shown in figure 2. The ^{18}F activity was 40 kBq ml^{-1}. The projection data were measured for 15 min at a gantry angle of 0°. The image reconstruction via the MLEM method was applied with the pixel size and slice thickness of 1.00 mm and a reconstruction volume of 15 × 15 × 15 cm^3.

2.5. Registration experiments

2.5.1. PDRI registration. PDRI registration was performed by comparing the in-plane digitally reconstructed planar image from the BOLPs and the image obtained from a conventional PET (Discovery ST, General Electric, Schenectady, New York). The pixel size and slice thickness were 3.91 and 3.27 mm, respectively. We placed the tumor phantom in a conventional PET such that the polycarbonate plate was parallel to the longitudinal axis and the center of the plate aligned with the isocenter. Data collection was performed for 15 min.

The tumor phantom was then placed at the isocenter of the BOLPs to obtain the data for the PDRI. Data were also collected for two additional conditions where the tumor phantom was displaced by 2 and 7 mm along the *Y*-axis, away from the isocenter to avoid the observer's bias from trial learning. Each measurement with the BOLPs was carried out for 5 min. The activity of ^{18}F was 20 kBq ml^{-1} and the background activity was 4 kBq ml^{-1}. The gantry angle was fixed at 0°. MLEM image reconstruction was applied with the pixel size and slice thickness of 1.00 mm and a reconstruction volume of 15 × 15 × 5 cm^3. PDRIs corresponding

to 1, 3 and 5 min measurements were generated for each setup position. Image registration based on the PDRI for each setup position was performed by five observers. The reference image was reconstructed from a conventional PET image.

2.5.2. Radiographic registration. To compare the accuracy of radiographic and PDRI registrations, we also performed image registration using images obtained from an x-ray CT and a fluoroscopic system. The tumor phantom was placed at the isocenter of the x-ray CT following the same setup as used in the PET measurement. The pixel size and slice thickness were 0.98 and 1.25 mm, respectively. Fluoroscope images of the tumor phantom were also taken using the installed fluoroscopic system in the proton irradiation system. The position of the tumor phantom was subsequently moved along the Y-axis to take additional data at 2 and 7 mm from the isocenter. The reference image used in the radiographic registration was the DRR reconstructed from x-ray CT.

2.5.3. Registration accuracy evaluation. To evaluate the accuracy of the registration methods, image registration trials using in-house software were performed for ten trials. Each trial consisted of five different images shown twice to the observers. Five observers estimated the shifts in each trial. From the image registration data, we calculated the registration error (RE) using equation (1). Actual shift (Y_{actual}) was 0, 2 and 7 mm along the Y-axis. Z_{obs} and Y_{obs} in the equation refer to the observed translation along the Z-axis and Y-axis respectively performed by the five subjects. Statistical analysis was performed based on the registration error for both the radiographic and PDRI registrations:

$$\text{RE(mm)} = \sqrt{(Z_{\text{obs}})^2 + (Y_{\text{obs}} - Y_{\text{actual}})^2}. \tag{1}$$

Here RE denotes the registration error, Z_{obs} the observed translation along the Z-axis, Y_{obs} the observed translation along the Y-axis and Y_{actual} the actual setup couch translation along the Y-axis (0, 2, 7 mm).

2.5.4. Statistical analysis. Statistical analysis of our data was performed using JMP 8 (SAS Institute Inc.) software. The mean registration error and standard deviation (SD) for the various diameters were determined based on the acquisition time for data collection (i.e. 1, 3 and 5 min) and modality (BOLPs, x-ray fluoroscopy). Data were analyzed by one-way ANOVA, while the differences among means were analyzed by two-sided Student's t-test with the level of statistical significance set to $p < 0.05$.

3. Results

3.1. FWHM of the profile of 2 mm diameter sources

Figure 4 shows the reconstructed in-plane and cross-plane images of the cylindrical phantom corresponding to a gantry angle of 0°. The reconstructed source diameter at the central position was larger than the others due to blurring caused by adjacent sources. The FWHM of each radiation source is shown in figure 5. The mean ± SD for FWHM was 1.8 ± 0.3 mm in the in-plane image and 8.1 ± 1.2 mm in the cross-plane image at a gantry angle of 0°.

3.2. Registration accuracy evaluation

Shown in figure 6 are the PDRIs of the tumor phantom at a gantry angle of 0°. Images from left to right correspond to the three acquisition times (1, 3 and 5 min) for data collection,

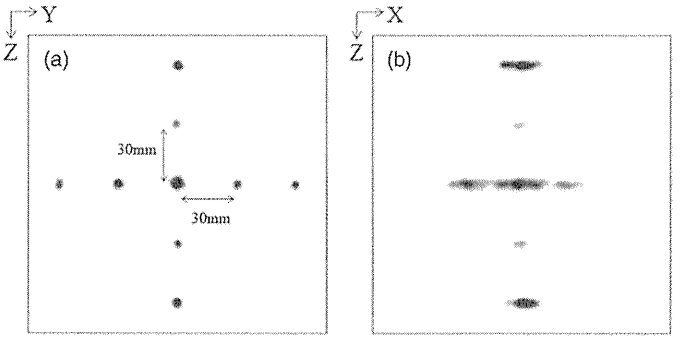

Figure 4. Planar images of the ^{18}F-sources along the (a) in-plane and (b) cross-plane directions reconstructed from the BOLPs data at a gantry angle of 0°.

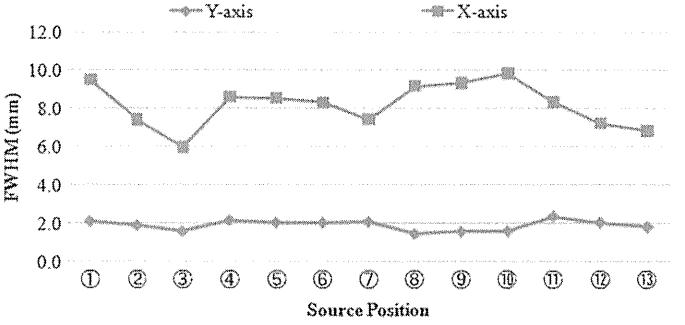

Figure 5. FWHM of the profile of the 2 mm diameter sources in the cylindrical phantom of figure 2.

while those from top to bottom correspond to the positions of the phantom (0, 2 and 7 mm) during data acquisition. The gray-scale window level of the images was adjusted to enhance the contrast. The measured activity at the source increased linearly as a function of acquisition time, and contrast to the background was constant and no inconsistency was observed among the three positions.

Figure 7 shows the variations in the observed PDRI and radiographic registration errors with respect to the acquisition time, phantom position and source diameter. PDRI registration errors were obtained from the registration of the reconstructed PET and BOLPs planar images. The radiographic registration errors were obtained from registration of DRR and portal (x-ray) images. The dependence of the registration error on the phantom position was not seen for each diameter.

Shown in table 1 are the mean ± SD of the registration errors based on our ANOVA. For the diameter of 8 mm the mean registration error of the PDRI registration appears to be influenced by the acquisition time with the longest acquisition time having the least mean registration error. The registration error for the radiographic registration was comparable to that of the shortest acquisition time of 1 min for the PDRI. The differences in the registration error between the image registration modalities listed in table 1 for the 8 mm diameter were found to be significant at a p-value of <0.0001. On the other hand, the mean registration error in all four registration methods for the diameter of 12 mm was found to be statistically insignificant ($p = 0.3545$) with their mean registration error ranging between 0.49 and 0.63. For diameters of 16 and 24 mm, the three acquisition times using the PDRI resulted in similar